

Journal Pre-proofs

Thermodynamic properties and rare-earth spectroscopy of $\text{Cu}_3\text{Nd}(\text{SeO}_3)_2\text{O}_2\text{X}$
(X = Cl, Br)

Maria M. Markina, Konstantin V. Zakharov, Peter S. Berdonosov, Valery A. Dolgikh, Elena S. Kuznetsova, Sergei A. Klimin, Oleg B. Yumashev, Alexander N. Vasiliev

PII: S0304-8853(19)32132-8
DOI: <https://doi.org/10.1016/j.jmmm.2019.165721>
Reference: MAGMA 165721

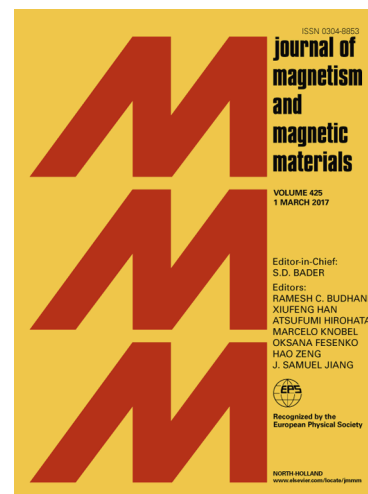
To appear in: *Journal of Magnetism and Magnetic Materials*

Received Date: 19 June 2019
Accepted Date: 18 August 2019

Please cite this article as: M.M. Markina, K.V. Zakharov, P.S. Berdonosov, V.A. Dolgikh, E.S. Kuznetsova, S.A. Klimin, O.B. Yumashev, A.N. Vasiliev, Thermodynamic properties and rare-earth spectroscopy of $\text{Cu}_3\text{Nd}(\text{SeO}_3)_2\text{O}_2\text{X}$ (X = Cl, Br), *Journal of Magnetism and Magnetic Materials* (2019), doi: <https://doi.org/10.1016/j.jmmm.2019.165721>

This is a PDF file of an article that has undergone enhancements after acceptance, such as the addition of a cover page and metadata, and formatting for readability, but it is not yet the definitive version of record. This version will undergo additional copyediting, typesetting and review before it is published in its final form, but we are providing this version to give early visibility of the article. Please note that, during the production process, errors may be discovered which could affect the content, and all legal disclaimers that apply to the journal pertain.

© 2019 Published by Elsevier B.V.



Thermodynamic properties and rare-earth spectroscopy of $\text{Cu}_3\text{Nd}(\text{SeO}_3)_2\text{O}_2\text{X}$ ($\text{X} = \text{Cl}, \text{Br}$)

Maria M. Markina,¹ Konstantin V. Zakharov,¹ Peter S. Berdonosov,¹ Valery A. Dolgikh,¹ Elena S. Kuznetsova,¹ Sergei A. Klimin,² Oleg B. Yumashev,³ Alexander N. Vasiliev^{1,4,5}*

¹Lomonosov Moscow State University, Moscow 119991, Russia

²Institute of Spectroscopy, RAS, Troitsk 142190, Russia

³Institute of Applied Mechanics, RAS, Moscow 125040, Russia

⁴National University of Science and Technology “MISiS”, Moscow 119049, Russia

⁵National Research South Ural State University, Chelyabinsk 454080, Russia

KEYWORDS francisite, metamagnetic phase transition, kagome lattice, magnetic phase diagram, rare-earth spectroscopy.

The kagome lattice of copper ions in francisite-type compounds is quite sensitive to external stimuli, being easily affected by temperature and magnetic field. The rare-earth ions inserted between buckled layers of transition metal add new dimension to magnetism in these systems.

*vasil@mig.phys.msu.ru, +7(495)932-92-17

Neodymium francisites, $\text{Cu}_3\text{Nd}(\text{SeO}_3)_2\text{O}_2\text{X}$ ($\text{X} = \text{Cl}, \text{Br}$), experience long range magnetic order at $T_N = 34 \text{ K}$ (Cl) or 35.2 K (Br) and spin reorientation transition at $T_R = 4 \text{ K}$ (Cl) or 4.6 K (Br) marked by sharp anomalies in magnetization M , specific heat C_p , and optical spectra. The spin reorientation of Cu^{2+} ions is due to d - f interaction of transition and rare-earth magnetic subsystems. Under action of modest external field $B < 2 \text{ T}$ both compounds exhibit metamagnetic phase transition, largely hysteretic in case of Cl compound at $T < T_R$.

Introduction

Low dimensional and frustrated magnetic systems attract immense attention due to the rich palette of ordered and disordered quantum ground states.¹ Exotic phases realized at low temperatures include gapped² and gapless³ spin liquids, skyrmions⁴ and Z2 vortices,⁵ non-trivial long-range ordered structures,⁶ etc. Among this multitude, the francisite mineral, $\text{Cu}_3\text{Bi}(\text{SeO}_3)_2\text{O}_2\text{Cl}$, is notable owing to its six-sublattices non-collinear antiferromagnetic spin arrangement. The crystal structure of natural francisite initially has been described in mineral science.⁷⁻¹⁰ First rare-earth substituted compound, $\text{Cu}_3\text{Er}(\text{SeO}_3)_2\text{O}_2\text{Cl}$, isostructural to the pristine one was synthesized soon afterwards.¹¹

Basic physical properties of synthetic $\text{Cu}_3\text{Bi}(\text{SeO}_3)_2\text{O}_2\text{X}$ ($\text{X} = \text{Cl}, \text{Br}$) were established in pioneering work of Millet et al.¹² Sharp anomalies in magnetic susceptibility were detected in Cl and Br compounds at comparable temperatures $T_N \sim 24 \text{ K}$, albeit authors claimed “...no evidence for a magnetically ordered state at low temperatures”. Besides, additional anomalies in linear birefringence at about $T_s \sim 125 \text{ K}$ were seen in both Cl and Br species ascribed to unidentified structural phase transition. Finally, two series of Cl and Br rare-earth francisite-type compounds

were systematically synthesized confirming their orthorhombic crystal structure, space group $Pm\bar{m}n$.¹³ No similar compounds with tellurium were found. Overall, about twenty five Cl and Br francisite-type compound were reported ($\text{Cu}_3\text{Bi}(\text{SeO}_3)_2\text{O}_2\text{I}$ unconfirmed) most being virtually uninvestigated in physical measurements.¹⁴

Magnetic structure of $\text{Cu}_3\text{Bi}(\text{SeO}_3)_2\text{O}_2\text{Br}$ was solved by single-crystal neutron diffraction.¹⁵ Below $T_N = 27.4$ K, this compound is the layered antiferromagnet with six-sublattices canted ferrimagnetic spin arrangement. The non-collinearity of Cu^{2+} magnetic moments stems from the competition of multiple ferromagnetic and antiferromagnetic intralayer exchange interactions. The response of Br francisite to external magnetic field is quite anisotropic. At magnetic field $B \sim 0.8$ T applied along the c axis, i.e. perpendicular to ab layers, the system experiences sharp metamagnetic transition associated with a flip of every second magnetic layer. Much higher fields are needed to rotate the magnetization toward the b axis ($B \sim 7$ T) or the a axis ($B \sim 15$ T).¹⁵ These observations were analyzed and confirmed in the first principles study of the magnetic ground state of Cl and Br francisites.¹⁶ The doping of $\text{Cu}_3\text{Bi}(\text{Se}_{1-x}\text{Te}_x\text{O}_3)_2\text{O}_2\text{Cl}$ ($0 \leq x \leq 0.6$) polycrystalline samples was undertaken to further explore the metamagnetic phase transition.¹⁷

Further research on $\text{Cu}_3\text{Bi}(\text{SeO}_3)_2\text{O}_2\text{X}$ ($\text{X} = \text{Cl}, \text{Br}$) concentrated on antiferroelectric lattice distortion observed in Cl compound at $T_s = 115$ K and absent in its Br counterpart down to lowest temperatures. At phase transition, the orthorhombic space group $Pm\bar{m}n$ reduces to a lower symmetry space group $Pc\bar{m}n$ due the doubling of unit cell along the c axis. This phase transition was detected by high-resolution synchrotron powder diffraction,¹⁸ single crystal neutron diffraction,¹⁹ Raman scattering²⁰ and through measurements of various dielectric and thermal parameters.

The studies of yttrium²¹ and “non-magnetic” rare-earth francisites based on lanthanum,²² europium and lutetium²³ revealed similarity in their magnetic response to bismuth francisite albeit no signatures of antiferroelectric phase transition were seen in any of them. Interestingly, the room temperature crystal structure of Te substituted francisite, $\text{Cu}_3\text{Bi}(\text{TeO}_3)_2\text{O}_2\text{Cl}$, is isostructural with the low temperature phase of $\text{Cu}_3\text{Bi}(\text{SeO}_3)_2\text{O}_2\text{Cl}$.²⁴

The spin-flip-induced ferroelectricity was observed in measurements of dielectric constant and electric polarization in $\text{Cu}_3\text{Bi}(\text{SeO}_3)_2\text{O}_2\text{Cl}$ under action of external magnetic field.²⁵ This observation allows attributing the francisite to highly demanded multiferroic materials. Another practically important feature of francisite-type compounds concerns controllable broadband absorption observed in a multifrequency electron spin resonance study on $\text{Cu}_3\text{Bi}(\text{SeO}_3)_2\text{O}_2\text{Br}$.²⁶ Namely, the mixed phase stabilized in vicinity of metamagnetic transition at $B = 0.8$ T below T_N possesses an enhanced microwave absorption. This absorption is non-resonant showing no frequency dependence in the range 100–480 GHz.²⁷

New features in behavior of francisite-type compounds appear at “magnetic” rare-earth substitution of bismuth for samarium²⁸ and ytterbium.²⁹ Both compounds order magnetically at $T_N = 35$ K (Sm) or 36.7 K (Yb), but the interplay of rare-earth and transition metal subsystems results in spin-reorientation of Cu spins at $T_R \sim 9$ K. The infrared spectroscopy of rare-earth ions evidences splitting of the lowest-energy excited Kramers doublet at $T_R < T < T_N$ while the ground Kramers doublet splits only at $T < T_R$. Preliminary data on electronic spectra of rare-earth ions in $\text{Cu}_3\text{R}(\text{SeO}_3)_2\text{O}_2\text{Cl}$ (R = Sm, Yb, Er, Nd, Pr, Eu) represent the phase transitions being detected either by splitting of crystal-field doublets or by repulsion of crystal field levels in a staggered magnetic field.³⁰ Here, we report thermodynamic properties and rare-earth spectroscopy of $\text{Cu}_3\text{Nd}(\text{SeO}_3)_2\text{O}_2\text{X}$ (X = Cl, Br).

Synthesis and characterization

Francisite-type Nd compounds were obtained in sealed under vacuum quartz tubes from mixtures weighted according to equation: $5\text{CuO} + \text{CuX}_2 + \text{Nd}_2\text{O}_3 + 4\text{SeO}_2 = 2\text{Cu}_3\text{Nd}(\text{SeO}_3)_2\text{O}_2\text{X}$ ($\text{X} = \text{Cl}, \text{Br}$). All used commercially available reagents were at least 99% reagent grade. Selenium dioxide was obtained by dehydration of H_2SeO_3 (pure) under vacuum by heating in pump connected glass tube placed in boiling water. The decomposition product was sublimated in flow of dry air with NO_2 from lead nitrate decomposition. Reaction mixtures were heated in electronically controlled furnace at 300°C for 12–24 hrs and finally at 575°C for 72 hrs. At the end of the program the tubes were cooled with the furnace after switching off. Green powder samples were obtained. The powder XRD (Stoe Stadi-p, $\text{CuK}\alpha_1$) shows that francisite-type compounds were formed. The cell constants for $\text{Cu}_3\text{Nd}(\text{SeO}_3)_2\text{O}_2\text{Cl}$ ($a = 6.379(3) \text{ \AA}$, $b = 9.622(4) \text{ \AA}$, $c = 7.094(3) \text{ \AA}$, space group $Pm\bar{m}n$) have been found in a good agreement with data reported previously.¹³ Structure refinement for $\text{Cu}_3\text{Nd}(\text{SeO}_3)_2\text{O}_2\text{Br}$ was performed by Rietveld method on STOE Theta/Theta diffractometer using JANA 2006 software.³¹ The final refinement parameters and experimental data are summarized in Table 1. The Rietveld plot for $\text{Cu}_3\text{Nd}(\text{SeO}_3)_2\text{O}_2\text{Br}$ is shown in Fig. 1. The atomic coordinates and atomic displacement parameters are listed in Table 2. Interatomic distances are shown in Table 3. The crystal structure of $\text{Cu}_3\text{Nd}(\text{SeO}_3)_2\text{O}_2\text{X}$ ($\text{X} = \text{Cl}, \text{Br}$) is organized by buckled layers of corner-sharing CuO_6 octahedra. This network is strengthened additionally by SeO_3 triangles. The layers are coupled by Nd ions in octagonal environment while the chalcogen ions fill the channels in the structure.

Thermodynamic properties

Both *ac* and *dc* magnetic susceptibility χ and specific heat C_p were measured using relevant options of commercial “Quantum Design” MPMS-7T and PPMS-9T devices. The temperature

dependences of both real χ' and imaginary χ'' parts of *ac* magnetic susceptibility in $\text{Cu}_3\text{Nd}(\text{SeO}_3)_2\text{O}_2\text{X}$ ($\text{X} = \text{Cl}, \text{Br}$) taken at magnitude of exciting field 5 Oe and frequency 1000 Hz are shown in Fig. 2. The properties of these compounds differ in both paramagnetic and magnetically ordered states. In Cl system, real component χ' apparently follows the Curie-Weiss law and exhibit sharp anomaly at Neel temperature $T_N = 34$ K. Less pronounced anomaly at this temperature is seen in χ'' . The spin reorientation transition is marked by upturn in χ' and sharp peak in χ'' at $T_R = 4$ K. In Br system, χ' evidences low-dimensional behavior with correlation maximum most pronounced in χ'' at about 80 K. Two sharp anomalies in χ' mark Neel transition at $T_N = 35.2$ K and spin reorientation at $T_R = 4.6$ K. Imaginary component χ'' is insensitive to T_N , but exhibits sharp peak at T_R .

The temperature dependences of *dc* magnetic susceptibility $\chi = M/B$ in $\text{Cu}_3\text{Nd}(\text{SeO}_3)_2\text{O}_2\text{X}$ ($\text{X} = \text{Cl}, \text{Br}$) taken at various fields in zero-filled-cooled regime are shown in Fig. 3. Essentially, the static and dynamic data agree with each other though no sharp anomalies at either T_R or T_N can be detected under high magnetic field. The standard fitting of χ vs. T dependence by the Curie-Weiss law

$$\chi = \chi_0 + C/(T - \Theta). \quad (1)$$

is not possible for $\text{Cu}_3\text{Nd}(\text{SeO}_3)_2\text{O}_2\text{Br}$ due to pronounced correlation effects far above the Neel temperature. It can be done for $\text{Cu}_3\text{Nd}(\text{SeO}_3)_2\text{O}_2\text{Cl}$ however. From the data taken at $B = 0.1$ T in the range 150–300 K follow $\chi_0 = (1.06 \pm 0.07) \times 10^{-3}$ emu/mol, $C = 2.79 \pm 0.03$ emuK/mol and $\Theta = 18.9 \pm 0.8$ K. The large positive value of temperature independent term χ_0 should be attributed to van Vleck magnetism of Nd^{3+} ions which significantly exceeds the absolute value of the sum of diamagnetic Pascal constants³² of individual ions $\chi_{\text{dia}} = -1.88 \times 10^{-4}$ emu/mol. The Curie

constant C nicely corresponds to the sum of effective magnetic moments of 3Cu^{2+} ions ($S = 1/2$) and Nd^{3+} ions ($J = 9/2$, $g = 8/11$). The Weiss temperature Θ is positive indicating the predominance of ferromagnetic exchange interactions at elevated temperatures. Low value of Θ as compared to T_N signifies fierce competition of ferromagnetic and antiferromagnetic exchange interactions inherent for francisite-type compounds.

The field dependences of magnetization M in $\text{Cu}_3\text{Nd}(\text{SeO}_3)_2\text{O}_2\text{X}$ ($X = \text{Cl}, \text{Br}$) taken at various temperatures $T < T_N$ are shown in Fig. 4. Both compounds evidence the metamagnetic behavior distinctly different from “standard” spin-flop transition. Surprisingly, the value of magnetization reached in Br compound at highest field, $B = 9$ T, is almost triple of that in Cl compound. Besides, M vs. B curves taken at lowest temperature in these compounds are distinctly different at low magnetic field.

The difference in magnetic response of $\text{Cu}_3\text{Nd}(\text{SeO}_3)_2\text{O}_2\text{Cl}$ and $\text{Cu}_3\text{Nd}(\text{SeO}_3)_2\text{O}_2\text{Br}$ is evident in low temperature hysteretic loops, as shown in the insets to Fig. 4. The coercivity at $T < T_R$ is quite appreciable in Cl compound and it is vanishingly small in Br compound. The loop itself is quite peculiar combining features of both ferromagnetic and antiferromagnetic response. At $T_R < T < T_N$, both systems show no hysteresis but evidence sharp metamagnetic transition at $B_m \leq 2$ T. The value of B_m depends on temperature non-monotonously defining a boundary between antiferromagnetic and canted ferrimagnetic phases.

The findings in magnetization are further supported by the measurements of specific heat C_p . The temperature dependences of this property in $\text{Cu}_3\text{Nd}(\text{SeO}_3)_2\text{O}_2\text{X}$ ($X = \text{Cl}, \text{Br}$) are shown in Fig. 5. The phase transitions at T_R and T_N are marked by sharp anomalies clearly seen in C_p/T vs T representation, as shown in the Insets to Fig. 5. The comparable magnitudes of the anomalies at

spin order T_N and spin reorientation T_R transitions allows suggesting that both of them should be ascribed to the same magnetic subsystem, i.e. Cu^{2+} ions.

Optical spectroscopy

The infrared spectroscopy of $f-f$ transitions in Nd^{3+} ions has been performed to investigate further the magnetic phase transitions in $\text{Cu}_3\text{Nd}(\text{SeO}_3)_2\text{O}_2\text{X}$ ($\text{X} = \text{Cl}, \text{Br}$). We use the intrinsic property of the Kramers doublets to split in a magnetic field, no matter external or internal effective field \mathbf{B}_{eff} , acting on the rare-earth ion by the ordered subsystem of d -metal. Transmittance spectra in a wide spectral range 1800–15000 cm^{-1} have been taken using a Fourier–spectrometer Bruker IFS125HR. Mixtures of $\text{Cu}_3\text{Nd}(\text{SeO}_3)_2\text{O}_2\text{X}$ ($\text{X} = \text{Cl}$ or Br) and KBr powders were pressed into tablets with an effective thickness of francisite of about 10 μm . Low temperatures have been reached using an optical closed-cycle cryostat Cryomech PT403.

Several multiplets of Nd^{3+} ion ($^4\text{I}_{11/2}$, $^4\text{I}_{13/2}$, $^4\text{I}_{15/2}$, $^4\text{F}_{3/2}$, $^4\text{F}_{5/2}+^2\text{H}_{9/2}$, $^4\text{F}_{7/2}+^4\text{S}_{3/2}$) have been registered in the spectroscopic range studied. The scheme of Fig. 6a is to explain labeling of the transitions and the effect of magnetic field on Kramers doublets (KDs). In the crystal field (CF) the multiplets of the free ion split into the CF levels (marked as I, II, etc. for the ground $^4\text{I}_{9/2}$ multiplet and as A, B, etc. for the $^4\text{I}_{11/2}$ one). Optical transitions are marked by two labels corresponding to the initial and the final states of transitions, e.g., IA. In a magnetically ordered state KDs split depending on the anisotropy of the magnetic g -factors. In a general case, each spectral line splits into four lines, e.g., spectral line corresponding to the transition IA splits into the lines 1a, 1a', 1'a, and 1'a'. The transitions designated by dashed lines correspond to the spectral lines that “freeze out” at low temperatures due to the depopulation of the initial state of transition.

Temperature behaviour is typical for all the multiplets in both crystals under study, the Fig. 6b-e demonstrates those for ${}^4I_{11/2}$ one. This multiplet is split by a crystal field into $J + \frac{1}{2} = 6$ Kramers doublets. Spectral lines IA – IF correspond to the transitions from the ground KD of the ground ${}^4I_{9/2}$ multiplet to the KDs of the ${}^4I_{11/2}$. Only KD “I” is populated at low enough temperatures, that’s why there are six transition at temperatures $T \leq 15$ K, while in the temperature range $T \geq 15$ K, the second (or, the “first excited”) level “II” of the ground multiplet with the energy 29 cm^{-1} is populated. Correspondingly, the lines denoted as IIA – IIF grow in intensity. With cooling in a whole temperature range investigated (300–4 K), shift of the spectral lines and growth of CF splitting denotes the fact of CF strengthening due to the diminishing of the Nd-O distances in the nearest environment of Nd^{3+} ion.

The most drastic changes take place in the spectra at the temperatures $T < T_N$. Spectral lines split as it is shown for the line IA in Figs. 6d,e. The reason for that is splitting of KDs. The Kramers degeneracy can be lifted only by the action of the magnetic field. Such a field appears in a crystal due to the AFM ordering of the copper magnetic subsystem. The low-energy components of the split lines IA and IB “freeze out” at low temperatures. This is unambiguous evidence for the fact that ground KD splits at T_N . Comparison of the spectra of the $X = \text{Cl}$ and $X = \text{Br}$ compounds allows concluding that the CF is very similar in both francisites as well as crystallographic parameters given above, small difference of which leads to small shift of CF level of the Nd^{3+} ion ($\sim 3 \text{ cm}^{-1}$ for the IA line, see Fig. 6d,e). The splitting of the line IA resembles each other in both compounds except (i) the temperature of magnetic ordering T_N which is ~ 1 K higher in $X = \text{Br}$ francisite in accordance with the data given above and (ii) the value of the splitting of the ground KD Δ_0 is a bit greater in $X = \text{Cl}$ compound (7.4 vs 6.2 cm^{-1} at 10 K).

Temperature dependence of the full width on a half-height (FWHH) for the IA line is given in Fig. 7 for both compounds together with the lineshapes at several temperatures for the $\text{Cu}_3\text{Nd}(\text{SeO}_3)_2\text{O}_2\text{Cl}$. All lineshapes are given in the same spectral region $1961\text{--}1981\text{ cm}^{-1}$. FWHW of the IA line in both compounds follows intrinsic dependence of diminishing with lowering the temperature till $T \sim 120\text{ K}$, while, after that it starts to grow till temperature close to the T_N . Then, visible splitting of the spectral line occurs and one can follow the FWHH of one of the line components. The most interesting is the growth of FWHW with lowering the temperature from $T \sim 120\text{ K}$ to T_N . It is known that in the vicinity of the phase transition the spectroscopic parameters can demonstrate unusual behavior due to the existence of the fluctuations and instabilities when the system is close to the phase transition (e.g., phonons are broadened at temperatures close to the structural phase transition).³³ This behavior can be regarded as a precursor of the phase transition.

In low-dimensional magnetic systems, which are the case of francisites, the spin correlations exist at temperatures well above the temperature of the magnetic ordering³⁴. These spin correlations form local fluctuating magnetic field \mathbf{B}_{eff} , splitting KDs locally. The so-called “tails” of line splitting in the case of Kramers ions can be found well above the T_N , especially in magnetically low-dimensional systems, and for Nd^{3+} ion they were registered in 1D magnets $\text{Nd}_2\text{BaNiO}_5$ ³⁵ at $T > 2T_N$ and $\text{Nd}_2\text{BaCuO}_5$ ³⁶ at $T > 5T_N$. So, the growth of the FWHH at $120\text{ K} > T > T_N$ in both francisites studied is caused by the “tail” of splittings of Nd^{3+} KDs by spin correlations. As was discussed above spin correlations is an intrinsic property of magnetic low-dimensional system³⁴, while, in francisites being 2D magnets, spin correlations can be caused by some specific magnetic state, namely, in $\text{Cu}_3\text{Bi}(\text{SeO}_3)_2\text{O}_2\text{Br}$ compound magnetic anisotropy could be strong enough to impose a quasi-2D XY behavior¹⁵ and can exhibit a unique feature - a

Kosterlitz–Thouless transition. At temperatures lower than 10 K, the FWHH of the IA line exhibits minor raise again which can be considered as a precursor of another, low-temperature, phase transition. This agrees with thermodynamic properties.

Summary

Magnetic phase diagrams of $\text{Cu}_3\text{Nd}(\text{SeO}_3)_2\text{O}_2\text{X}$ ($\text{X} = \text{Cl}, \text{Br}$) extracted from thermodynamic measurements are shown in Fig. 8. Four different phases can be distinguished in these diagrams. PM denotes paramagnetic phase at $T > T_N$, AFM is the antiferromagnetic phase at $T_R < T < T_N$ at $B < B_m$, CFM is the canted ferrimagnetic phase at $T_R < T < T_N$ at $B > B_m$, AFMR is the reoriented antiferromagnetic phase at $T < T_R$.

Rich magnetic phase diagram of $\text{Cu}_3\text{Nd}(\text{SeO}_3)_2\text{O}_2\text{X}$ ($\text{X} = \text{Cl}, \text{Br}$) stems from the presence and interaction of the rare-earth and transition metal subsystems. The temperature-induced spin-reorientation phase transition takes place in the absence of external magnetic field. This instability in the vicinity of liquid helium temperature may lead to enhanced broadband absorption of microwave radiation similar to that observed in pristine francisite at metamagnetic phase transition.

ACKNOWLEDGMENTS

Dr A.V. Olenov is gratefully acknowledged for help with $\text{Cu}_3\text{Nd}(\text{SeO}_3)_2\text{O}_2\text{Br}$ structure refinement. This work has been supported by the Ministry of Education and Science of the Russian Federation in the framework of Increase Competitiveness Program of NUST “MISiS” Grant No. K2-2017-084; by Act 211 of the Government of Russian Federation, Contracts No. 02.A03.21.0004 and No. 02.A03.21.0011. This work has been performed in partial fulfillment of

Russian Science Foundation grant RSF 02010 and RFBR grants 18-52-52005, 18-02-00326, 17-02-00135.

REFERENCES

1. Vasiliev, A.; Volkova, O.; Zvereva, E.; Markina, M. Milestones of low-D quantum magnetism. *NPJ Quantum Materials* **2018**, *3*, 18. DOI: <https://doi.org/10.1038/s41535-018-0090-7>
2. Yan S.M.; Huse D.A.; White S.R. Spin-liquid ground state of the $S = 1/2$ kagome Heisenberg antiferromagnet. *Science* **2011**, *332* (6034), 1173-1176. DOI: [10.1126/science.1201080](https://doi.org/10.1126/science.1201080)
3. Wen X.G. Quantum orders and symmetric spin liquids. *Phys. Rev. B* **2002**, *65* (16), 165113. DOI: <https://doi.org/10.1103/PhysRevB.65.165113>
4. Muehlbauer S.; Binz B.; Jonietz F.; Pfleiderer C.; Rosch C.; Neubauer A.; Georgii R.; Boeni P. Skyrmion lattice in a chiral magnet. *Science* **2009**, *323* (5916), 915-919. DOI: [10.1126/science.1166767](https://doi.org/10.1126/science.1166767)
5. Nayak C.; Shtengel K. Microscopic models of two-dimensional magnets with fractionalized excitations. *Phys. Rev. B* **2001**, *64* (6), 064422. DOI: <https://doi.org/10.1103/PhysRevB.64.064422>
6. Grohol D.; Matan K.; Cho J.H.; Lee S.H.; Lynn J.W.; Nocera D.G.; Lee Y.S. Spin chirality on a two-dimensional frustrated lattice. *Nature Materials* **2005**, *4* (4), 323-328. DOI: <https://doi.org/10.1038/nmat1353>

7. Pring A.; Gatehouse B.M.; Birch W.D. Francisite, $\text{Cu}_3\text{Bi}(\text{SeO}_3)_2\text{O}_2\text{Cl}$, a new mineral from Iron-Monarch, South Australia – description and crystal structure. *Amer. Miner.* **1990**, *75* (11-12), 1421-1425. URL: <http://www.minsocam.org/MSA/AmMin/TOC/>
8. Mandarino J.A. Natural and synthetic selenites and selenates and their Gladstone-Dale compatibility. *Eur. J. Miner.* **1994**, *6* (3), 337-349. DOI: 10.1127/ejm/6/3/0337
9. Krivovichev S.V.; Starova G.L.; Filatov S.K. ‘Face-to-face’ relationships between oxocentred tetrahedral and cation-centred tetrahedral oxoanions in crystal structures of minerals and inorganic compounds. *Miner. Magazine* **1999**, *63* (2), 263-266. DOI: 10.1180/002646199548376
10. Nazarchuk E.V.; Krivovichev S.V.; Pankratova O.Y.; Filatov S.K. Thermal expansion of francisite, $[\text{Cu}_3\text{BiO}_2](\text{SeO}_3)_2\text{Cl}$, and its interpretation based on oxocentered copper-bismuth tetrahedra. *Phys. Chem. Miner.* **2000**, *27* (6), 440-444. DOI: <https://doi.org/10.1007/s002699900079>
11. Berrigan R.; Gatehouse B.M. $\text{Cu}_3\text{Er}(\text{SeO}_3)_2\text{O}_2\text{Cl}$, the erbium analogue of francisite. *Acta Cryst. C* **1996**, *52* (3), 496-497. DOI: <https://doi.org/10.1107/S0108270195014120>
12. Millet P.; Bastide B.; Pashchenko V.; Gnatchenko S.; Gapon V.; Ksari Y.; Stepanov A. Syntheses, crystal structures and magnetic properties of francisite compounds $\text{Cu}_3\text{Bi}(\text{SeO}_3)_2\text{O}_2\text{X}$ (X = Cl, Br and I). *J. Mater. Chem.* **2001**, *11* (4), 1152-1157. DOI:10.1039/B003682J

13. Berdonosov P.S.; Dolgikh V.A. Copper lanthanide selenite oxohalides with francisite structure: Synthesis and structural characteristics. *Russ. J. Inorg. Chem.* **2008**, *53* (9) 1353-1358. DOI: <https://doi.org/10.1134/S0036023608090027>
14. Berdonosov P.S.; Kuznetsova E.S.; Dolgikh V.A. Transition metal selenite halides: A fascinating family of magnetic compounds. *Crystals* **2018**, *8* (4), 159. DOI: <https://doi.org/10.3390/cryst8040159>
15. Pregelj M.; Zaharko O.; Gunther A.; Loidl A.; Tsurkan V.; Guerrero S. Magnetic ground state and two-dimensional behavior in pseudo-kagome layered system $\text{Cu}_3\text{Bi}(\text{SeO}_3)_2\text{O}_2\text{Br}$. *Phys. Rev. B* **2012**, *86* (14), 144409. DOI: <https://doi.org/10.1103/PhysRevB.86.144409>
16. Nikolaev S.A., Mazurenko V.V.; Tsirlin A.A.; Mazurenko V.G. First-principles study of the magnetic ground state and magnetization process of the kagome francisites $\text{Cu}_3\text{Bi}(\text{SeO}_3)_2\text{O}_2\text{X}$ ($\text{X} = \text{Cl}, \text{Br}$). *Phys. Rev. B* **2016**, *94* (14), 144412. DOI: <https://doi.org/10.1103/PhysRevB.94.144412>
17. Wu H.C.; Tseng W.J.; Yang P.Y.; Chandrasekhar K.D.; Berger H.; Yang H.D. Anisotropic pressure effects on the Kagome $\text{Cu}_3\text{Bi}(\text{SeO}_3)_2\text{O}_2\text{Cl}$ metamagnet. *J. Phys. D – Appl. Phys.* **2017**, *50* (26), 265002. DOI: <https://doi.org/10.1088/1361-6463/aa7491>
18. Prishchenko D.A.; Tsirlin A.A.; Tsurkan V.; Loidl A.; Jesche A.; Mazurenko V.G. Antiferroelectric instability in the kagome francisites $\text{Cu}_3\text{Bi}(\text{SeO}_3)_2\text{O}_2\text{X}$ ($\text{X} = \text{Cl}, \text{Br}$). *Phys. Rev. B* **2017**, *95* (6), 064102. DOI: <https://doi.org/10.1103/PhysRevB.95.064102>

19. Constable E.; Raymond S.; Petit S.; Ressoushe E.; Bourdarot F.; Debray J.; Josse, M.; Fabelo O.; Berger H.; de Brion S.; Simonet V. Magnetic and dielectric order in the kagome like francisite $\text{Cu}_3\text{Bi}(\text{SeO}_3)_2\text{O}_2\text{Cl}$. *Phys. Rev. B* **2017**, *96* (1), 014413. DOI: <https://doi.org/10.1103/PhysRevB.96.014413>
20. Gnezdilov V.; Pashkevich Yu.; Lemmens P.; Kurnosov V.; Berdonosov P.; Dolgikh V.; Kuznetsova E.; Pryadun V.; Zakharov K.; Vasiliev A. Lattice and magnetic instabilities in $\text{Cu}_3\text{Bi}(\text{SeO}_3)_2\text{O}_2\text{X}$ ($\text{X} = \text{Cl}, \text{Br}$). *Phys. Rev. B* **2017**, *96* (11), 115144. DOI: <https://doi.org/10.1103/PhysRevB.96.115144>
21. Zakharov K.V.; Zvereva E.A.; Berdonosov P.S.; Kuznetsova E.S.; Dolgikh V.A.; Clark L.; Black C.; Lightfoot P.; Kockelmann W.; Pchelkina Z.V.; Streltsov S.V.; Volkova O.S.; Vasiliev A.N. Magnetic order and spin model of the buckled kagome lattice material $\text{Cu}_3\text{Y}(\text{SeO}_3)_2\text{O}_2\text{Cl}$. *Phys. Rev. B* **2014**, *90* (21), 214417. DOI: <https://doi.org/10.1103/PhysRevB.90.214417>
22. Markina M.M.; Zakharov K.V.; Zvereva E.A.; Denisov R.S.; Berdonosov P.S.; Dolgikh V.A.; Kuznetsova E.S.; Olenev A.V.; Vasiliev A.N. Static and dynamic magnetic properties of two synthetic francisites $\text{Cu}_3\text{La}(\text{SeO}_3)_2\text{O}_2\text{X}$ ($\text{X} = \text{Br}$ and Cl). *Phys. Chem. Minerals* **2017**, *44* (4), 277-285. DOI: <https://doi.org/10.1007/s00269-016-0855-0>
23. Zakharov K.V.; Zvereva E.A.; Kuznetsova E.S.; Berdonosov P.S.; Dolgikh V.A.; Markina M.M.; Olenev A.V.; Shakin A.A.; Volkova O.S.; Vasiliev A.N. Two new lanthanide members of francisite family $\text{Cu}_3\text{Ln}(\text{SeO}_3)_2\text{O}_2\text{Cl}$ ($\text{Ln} = \text{Eu}, \text{Lu}$). *J. Alloys Compounds* **2016**, *685*, 442-447. DOI: <https://doi.org/10.1016/j.jallcom.2016.05.213>

24. Becker R.; Johnsson M. Crystal structure of $\text{Cu}_3\text{Bi}(\text{TeO}_3)_2\text{O}_2\text{Cl}$: a kagome lattice type compound. *Solid State Sci.* **2005**, *7* (4), 375-380. DOI: <https://doi.org/10.1016/j.solidstatesciences.2004.10.045>
25. Wu H.C.; Chandrasekhar K.D.; Yuan J.K.; Huang J.R.; Lin J.Y.; Berger H.; Yang H.D. Anisotropic spin-flip-induced multiferroic behavior in kagome $\text{Cu}_3\text{Bi}(\text{TeO}_3)_2\text{O}_2\text{Cl}$. *Phys. Rev. B* **2017**, *95* (12), 125121. DOI: <https://doi.org/10.1103/PhysRevB.95.125121>
26. Pregelj M.; Zaharko O.; Zorko A.; Gomilsek M.; Sendetskyi O.; Guenther A.; Ozerov M.; Zvyagin S.A.; Luetkens H.; Baines C.; Tsurkan V.; Loidl A. Controllable broadband absorption in the mixed phase of metamagnets. *Adv. Funct. Mater.* **2015**, *25* (24), 3634-3640. DOI: <https://doi.org/10.1002/adfm.201500702>
27. Zorko A.; Gomilsek M.; Pregelj M.; Ozerov M.; Zvyagin S.A.; Ozarovski A.; Tsurkan V.; Loidl A.; Zaharko O. Electron spin resonance insight into broadband absorption of the $\text{Cu}_3\text{Bi}(\text{SeO}_3)_2\text{O}_2\text{Br}$ metamagnet. *AIP Advances* **2016**, *6* (5), 056210. DOI: <https://doi.org/10.1063/1.4943534>
28. Zakharov K.V.; Zvereva E.A.; Markina M.M.; Stratan M.I.; Kuznetsova E.S.; Dunaev S.F.; Berdonosov P.S.; Dolgikh V.A.; Olenev A.V.; Klimin S.A.; Mazaev L.S.; Kashchenko M.A.; Ahmed M.A.; Banerjee A.; Bandyopadhyay S.; Iqbal A.; Rahaman B.; Saha-Dasgupta T.; Vasiliev A.N. Magnetic, resonance and optical properties of $\text{Cu}_3\text{Sm}(\text{SeO}_3)_2\text{O}_2\text{Cl}$: a rare earth francisite compound. *Phys. Rev. B* **2016**, *94* (5), 054401. DOI: <https://doi.org/10.1103/PhysRevB.94.054401>
29. Markina M.M.; Zakharov K.V.; Ovchenkov E.A.; Berdonosov P.S.; Dolgikh V.A.; Kuznetsova E.S.; Olenev A.V.; Klimin S.A.; Kashchenko M.A.; Budkin I.V.; Yatsyk

- I.V.; Demidov A.A.; Zvereva E.A.; A.N. Vasiliev. Interplay of rare-earth and transition metal subsystems in $\text{Cu}_3\text{Yb}(\text{SeO}_3)_2\text{O}_2\text{Cl}$. *Phys. Rev. B* **2017**, *96* (13), 134422. DOI: <https://doi.org/10.1103/PhysRevB.96.134422>
30. Klimin S.A.; Budkin I.V. Magnetic phase transitions in two-dimensional frustrated $\text{Cu}_3\text{R}(\text{SeO}_3)_2\text{O}_2\text{Cl}$. Spectroscopic study. *EPJ Web of Conferences* **2017**, *132*, 02010. DOI: <https://doi.org/10.1051/epjconf/201713202010>
31. Petricek V.; Dusek M.; Palatinus L. Crystallographic computing system JANA2006: General features. *Z. Kristallogr.* **2014**, *229* (5), 345-352. DOI: <https://doi.org/10.1515/zkri-2014-1737>
32. Bain G.A.; Berry J.F. Diamagnetic corrections and Pascal's constants. *J. Chem. Educ.* **2008**, *85* (4), 532-536. DOI: [10.1021/ed085p532](https://doi.org/10.1021/ed085p532)
33. Klimin S.A., Kuzmenko A.B., Kashchenko M.A., and Popova M.N., Infrared study of lattice dynamics and spin-phonon and electron-phonon interactions in multiferroic $\text{TbFe}_3(\text{BO}_3)_4$ and $\text{GdFe}_3(\text{BO}_3)_4$, *Phys. Rev. B*, **2016**, *93* (5), 054304. DOI: <https://doi.org/10.1103/PhysRevB.93.054304>
34. de Jong L.J., Miedema A.R., Experiments on simple magnetic model systems, *Adv. Phys.* **1974**, *23* (1), 1. DOI: <https://doi.org/10.1080/00018739700101558>
35. Popova E.A., Klimin S.A., Popova M.N., Klingeler R., Tristan N., Büchner B., and Vasiliev A.N., Magnetic properties of quasi-one-dimensional antiferromagnets $(\text{Y}_{1-x}\text{Nd}_x)_2\text{BaNiO}_5$ ($x = 1, 0.15$). *J. Magn. and Magn. Materials* **2013**, *331*, 133. DOI: <https://doi.org/10.1016/j.jmmm.2012.11.019>

36. Popova M.N., Klimin S.A., Antic-Fidancev E., Porcher P., Optical and crystal-field Analysis of Nd^{3+} ion in $\text{Nd}_2\text{BaCuO}_5$ and $\text{Nd}_2\text{BaZnO}_5$, *J. of Solid State Chem.*, **2001**, 162 (1), 42. DOI: <https://doi.org/10.1006/jssc.2001.9339>

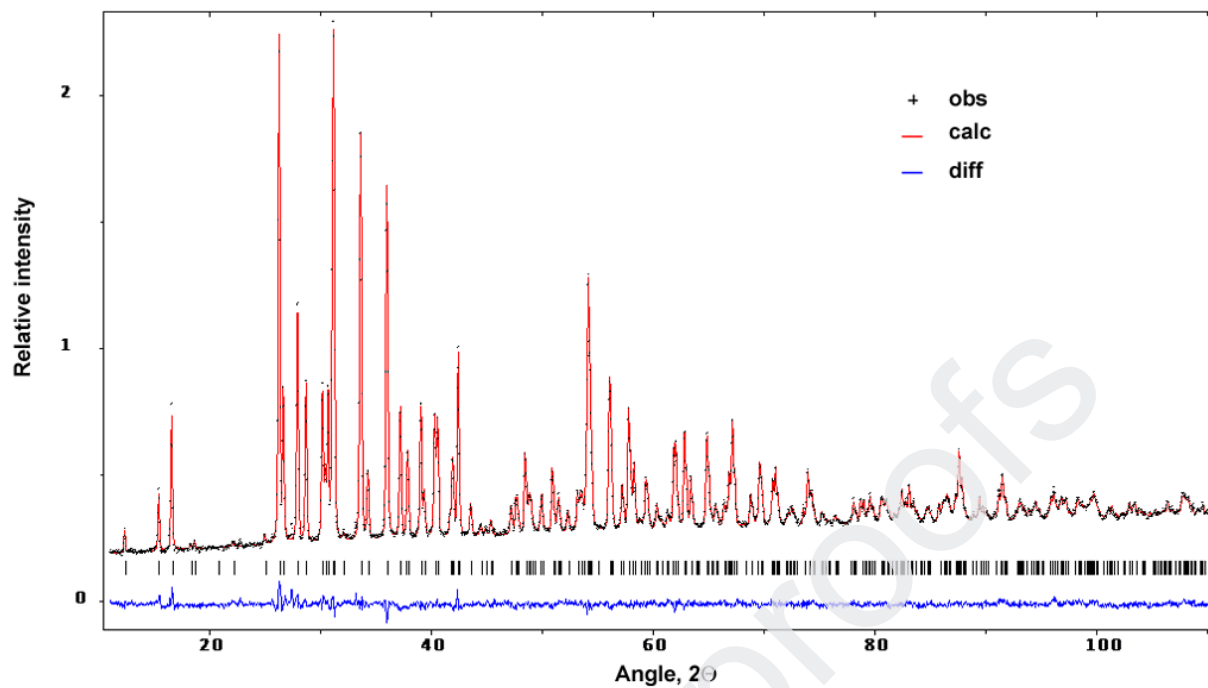


Figure 1. The Rietveld plot for $\text{Cu}_3\text{Nd}(\text{SeO}_3)_2\text{O}_2\text{Br}$.

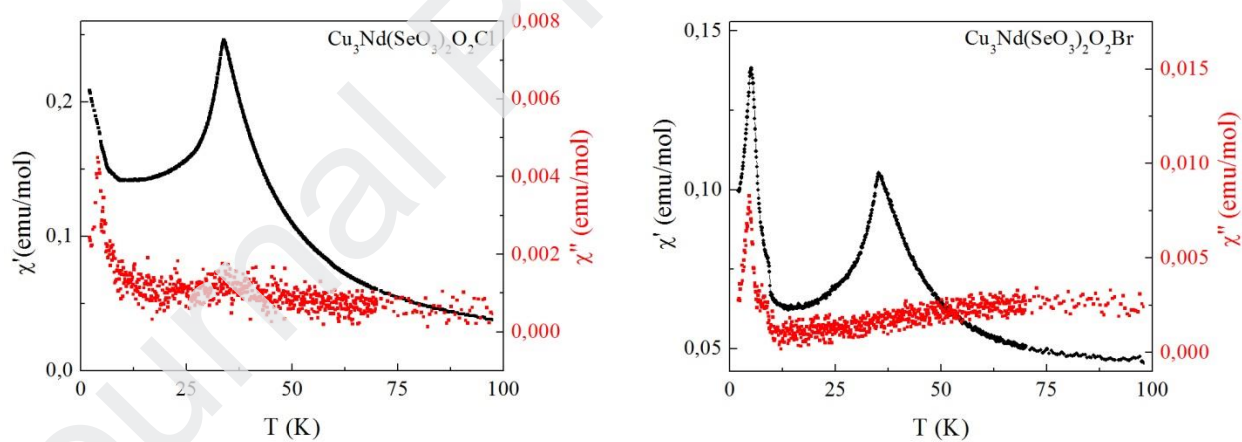


Figure 2. Temperature dependences of both real χ' and imaginary χ'' parts of *ac* magnetic susceptibility in $\text{Cu}_3\text{Nd}(\text{SeO}_3)_2\text{O}_2\text{Cl}$ (left panel) and $\text{Cu}_3\text{Nd}(\text{SeO}_3)_2\text{O}_2\text{Br}$ (right panel).

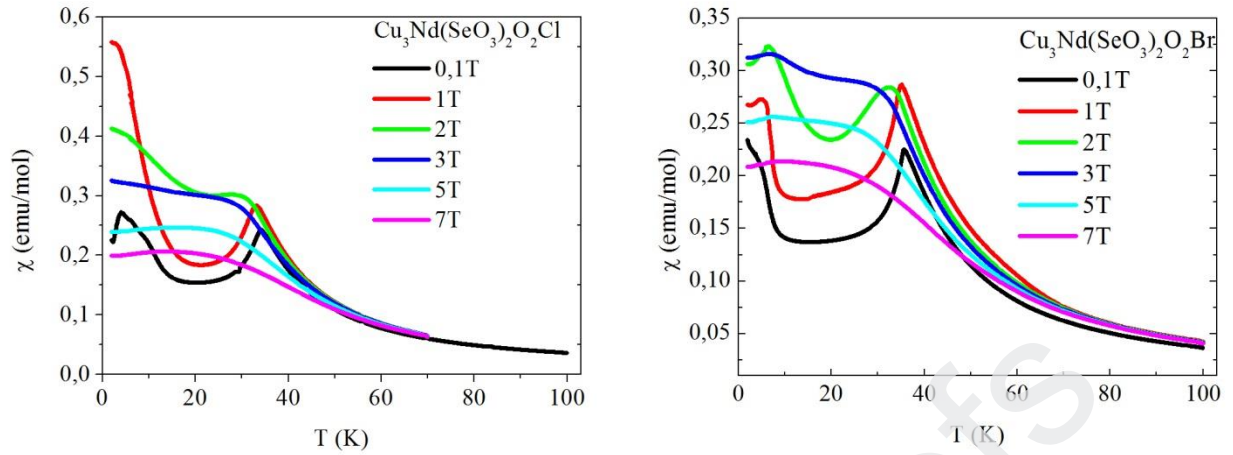


Figure 3. Temperature dependences of *dc* magnetic susceptibility at various magnetic fields in $\text{Cu}_3\text{Nd}(\text{SeO}_3)_2\text{O}_2\text{Cl}$ (left panel) and $\text{Cu}_3\text{Nd}(\text{SeO}_3)_2\text{O}_2\text{Br}$ (right panel).

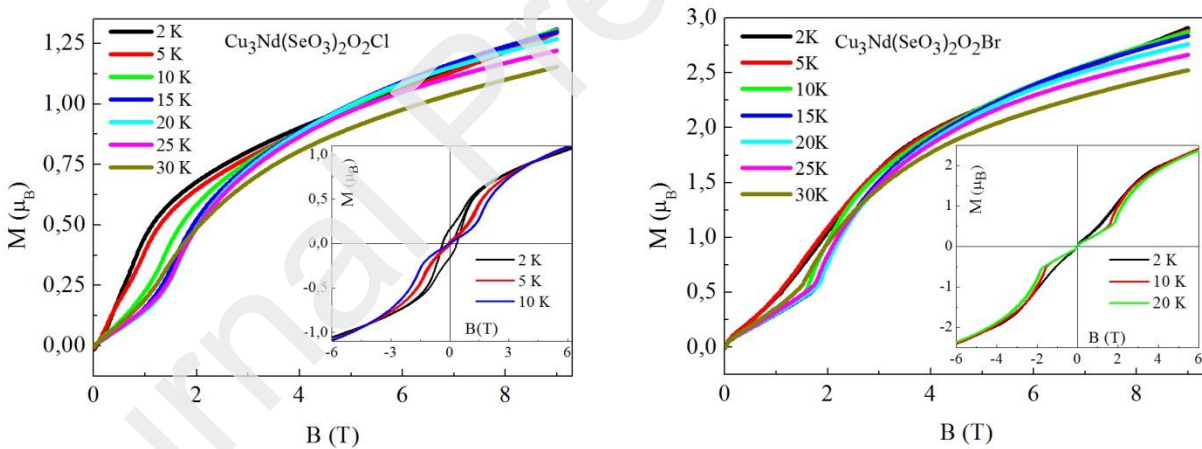


Figure 4. Magnetic field dependences of magnetization M at various temperatures in $\text{Cu}_3\text{Nd}(\text{SeO}_3)_2\text{O}_2\text{Cl}$ (left panel) and $\text{Cu}_3\text{Nd}(\text{SeO}_3)_2\text{O}_2\text{Br}$ (right panel). Insets: Hysteretic loops in magnetization of $\text{Cu}_3\text{Nd}(\text{SeO}_3)_2\text{O}_2\text{Cl}$ (left panel) and $\text{Cu}_3\text{Nd}(\text{SeO}_3)_2\text{O}_2\text{Br}$ (right panel) at low temperatures.

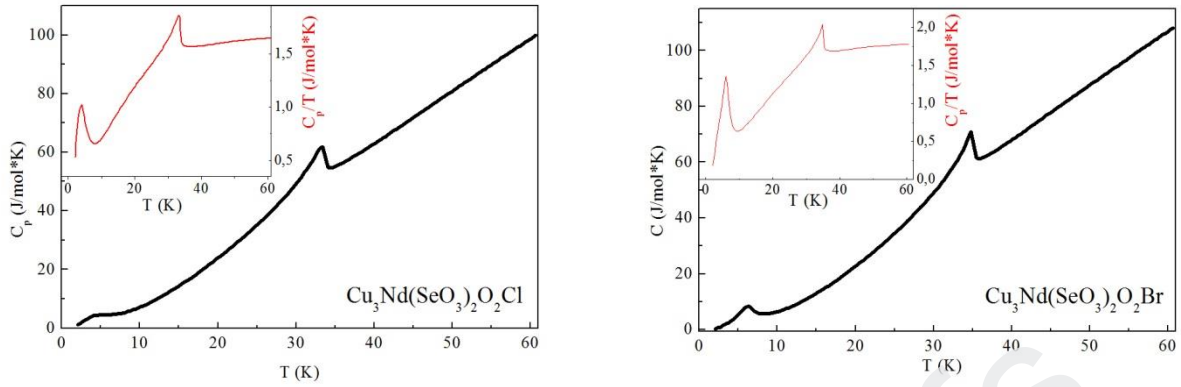


Figure 5. Temperature dependences of specific heat in $\text{Cu}_3\text{Nd}(\text{SeO}_3)_2\text{O}_2\text{Cl}$ (left panel) and $\text{Cu}_3\text{Nd}(\text{SeO}_3)_2\text{O}_2\text{Br}$ (right panel). The insets represent C_p/T vs. T curves.

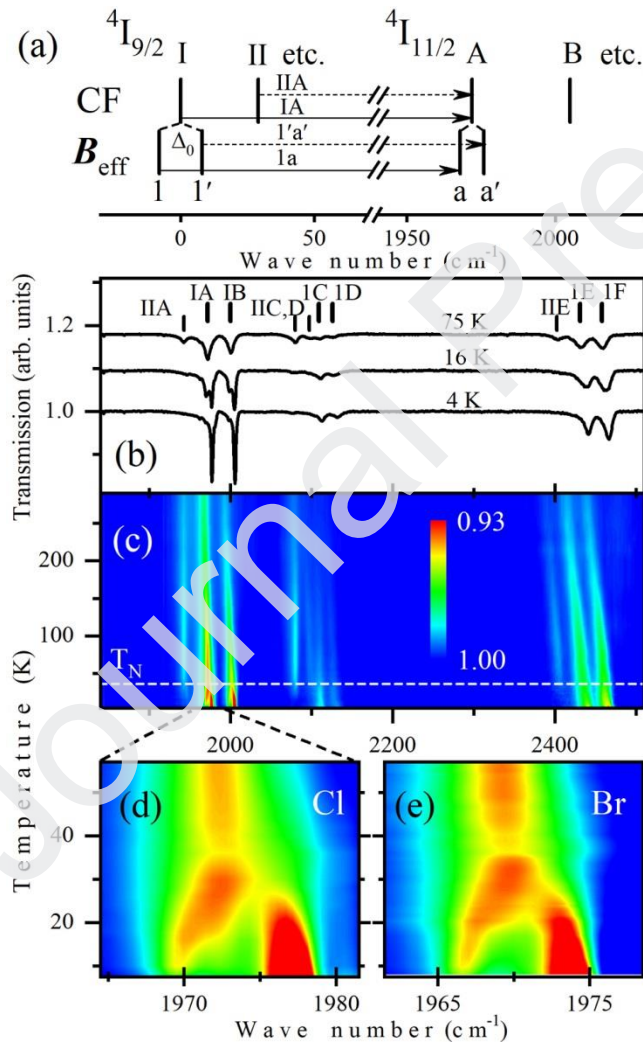


Figure 6. (a) Energy level scheme. (b,c) Multiplet ${}^4I_{11/2}$ of the Nd^{3+} ion in $\text{Cu}_3\text{Nd}(\text{SeO}_3)_2\text{O}_2\text{Cl}$ as (b) transmission spectra at various temperatures, and (c) color map. (d,e) Color maps in the region of the lowest-frequency spectral line IA of the multiplet for (d) $X = \text{Cl}$ (e) $X = \text{Br}$.

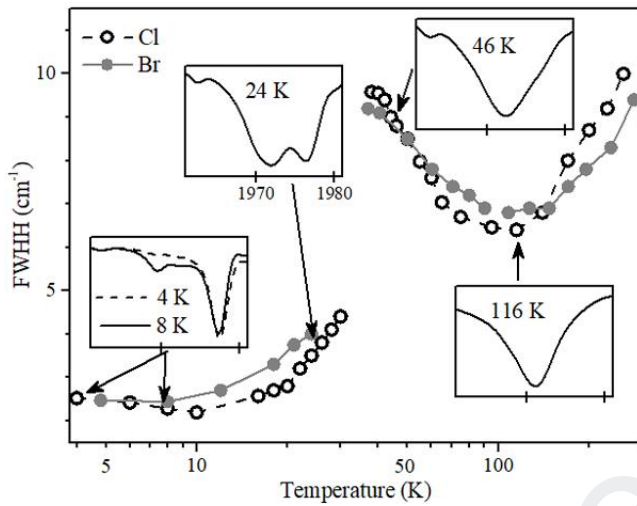


Figure 7. The temperature dependence of the full width on the half-height (FWHH) of the IA line of the $\text{Nd}^{3+} {}^4I_{11/2}$ multiplet in both compounds. Insets show the evolution of the lineshapes with temperature in the same spectral region (shown for $T = 24$ K) of the IA line for the Cl compound.

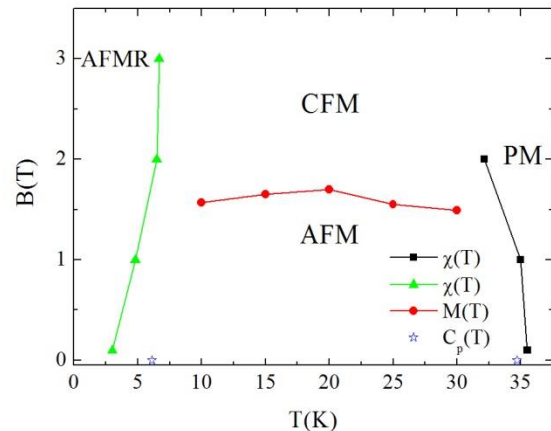
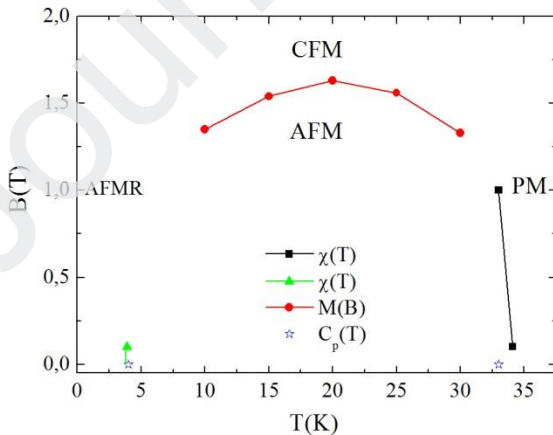


Figure 8. Magnetic phase diagrams of $\text{Cu}_3\text{Nd}(\text{SeO}_3)_2\text{O}_2\text{Cl}$ (left panel) and $\text{Cu}_3\text{Nd}(\text{SeO}_3)_2\text{O}_2\text{Br}$ (right panel). PM – paramagnetic phase, AFM – antiferromagnetic phase, AFMR – reoriented antiferromagnetic phase, CFM – canted ferrimagnetic phase.

Table 1. Rietveld refinement data for $\text{Cu}_3\text{Nd}(\text{SeO}_3)_2\text{O}_2\text{Br}$.

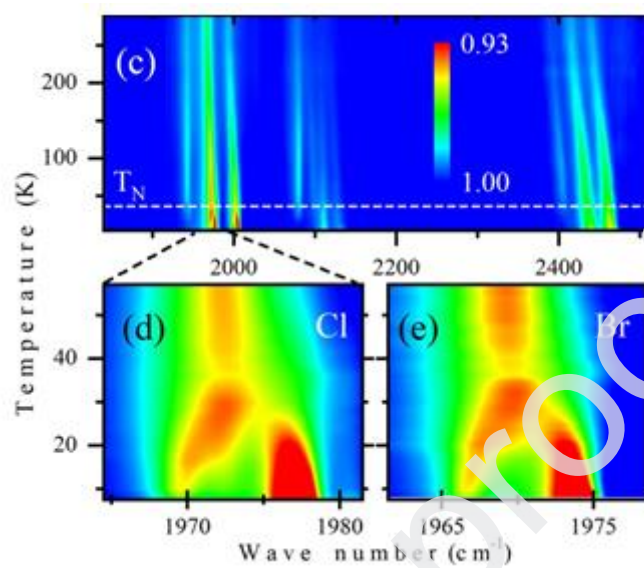
Symmetry	Orthorhombic
Space group	<i>Pmmn</i>
<i>a</i> , Å	6.36840(8)
<i>b</i> , Å	9.64497(14)
<i>c</i> , Å	7.10058(10)
<i>V</i> , Å ³	436.139(10)
<i>Z</i>	2
Density calc., g/cm ³	5.3339
Instrument	STOE theta/theta
Temperature, K	293
Wavelength, Å	1.5418
Software	JANA2006
Absorption coefficient, μ/mm	68.071
2θ range, °	11-110
R	0.0295
wR	0.0287
Goodness of fit	1.55

Table 2. Atomic coordinates and isotropic displacement parameters (in \AA^2) for $\text{Cu}_3\text{Nd}(\text{SeO}_3)_2\text{O}_2\text{Br}$.

Atom	Position	x	y	z	U	U ₁₁	U ₂₂	U ₃₃	U ₁₂	U ₁₃	U ₂₃
Nd1	2a	1/4	1/4	0.2664 (2)		0.0253 (12)	0.0248 (12)	0.0264 (13)	0	0	0
Cu1	4c	0	0	0		0.0406 (19)	0.041 (2)	0.043 (3)	-0.0079 (16)	0.0006 (19)	0.0014 (18)
Cu2	2a	1/4	1/4	0.7968 (5)		0.028 (3)	0.043 (3)	0.021 (3)	0	0	0
Se1	4e	1/4	0.5549 (2)	0.5971 (3)		0.0307 (17)	0.0301 (17)	0.0244 (15)	0	0	0.0043 (12)
Br1	2b	1/4	3/4	0.1531 (4)		0.041 (3)	0.052 (3)	0.047 (3)	0	0	0
O1	4e	1/4	0.1092 (12)	0.9999 (14)	0.038(4)						
O2	8g	0.0445 (11)	0.5803 (7)	0.7421 (11)	0.032(3)						
O3	4e	1/4	0.1191 (11)	0.5825 (15)	0.025(4)						

Table 3. Selected interatomic distances (Å) in $\text{Cu}_3\text{Nd}(\text{SeO}_3)_2\text{O}_2\text{Br}$.

Bond		Distance
Nd1—O1	x2	2.329(11)
Nd1—O2i	x4	2.490(7)
Nd1—O3	x2	2.575(11)
Cu1—O2	x2	2.008(8)
Cu1—O1	x2	1.909(6)
Cu2—O1	x2	1.981(11)
Cu2—O3	x2	1.977(11)
Se1—O3		1.681(11)
Se1—O2	x2	1.683(7)



Basic thermodynamic properties of Nd-francisites are reported

Rare-earth spectroscopy revealed the spin-reorientation

Magnetic phase diagrams of $\text{Cu}_3\text{Nd}(\text{SeO}_3)_2\text{O}_2\text{X}$ ($\text{X} = \text{Cl}, \text{Br}$) are established

Journal Pre-proofs